

Electromagnetic Field Tapering in the High-Roughness Substrates Coated by a Single Layer of Manganese: A Lithography-Free Approach to Ultra-Broadband, Wide-Angle, UV to IR Perfect Absorption

Majid Aalizadeh,^{1,2,*} Mohammad Reza Tavakkol,³ Amin Khavasi,³ Mehmet Yilmaz,⁴ Ekmel Ozbay^{1,2,4,5}

¹ Department of Electrical and Electronics Engineering, Bilkent University, Ankara 06800, Turkey

² Nanotechnology Research Center (NANOTAM), Bilkent University, Ankara 06800, Turkey

³ Electrical Engineering Department, Sharif University of Technology, Tehran, 11155-4363, Iran

⁴ National Nanotechnology Research Center (UNAM), Bilkent University, Ankara 06800, Turkey

⁵ Department of Physics, Bilkent University, Ankara 06800, Turkey

*majid.aalizadeh@bilkent.edu.tr

Abstract

Thick metallic layers are known to be used for the suppression of wave transmission through them. In this work, we propose an experimental facile and straightforward approach for using a thick single layer of the metal of Manganese (Mn) as both the transmission and reflection suppresser. This leads to obtaining lithography-free ultra-broadband perfect absorption in the ultra-wide spectrum ranging from Ultraviolet (UV) to Infrared (IR). The measured average absorption is approximately 99%. It is possible by only coating a thick layer of this metal on any high-roughness substrate that includes random tapered features on it. The key to this ultra-wideband absorption is the concept of Electromagnetic Field Tapering which enables the smooth and gradual impedance matching of the structure to the free space. This promising result is also attributed to the very appropriate-for-absorption optical properties of Mn. A full experimental characterization of the fabricated sample is presented along with the physical analysis of the phenomena. The findings of this paper can be used for the realization of lithography-free, cost-effective and high-throughput mass production of such broadband absorbers.

Keywords: Electromagnetic Field Tapering, Manganese, gradual impedance matching, Ultra-broadband absorption

Introduction

Broadband absorbers are increasingly attracting attention, because of their wide range of applications including photovoltaics [1-4], thermal emission [5], photodetection [6-10], thermal imaging [11-13], shielding [14,15], etc. Metamaterials have made it possible to create subwavelength broadband absorbers feasible for optical circuit integration. In such cases, generally the structure consists of a thick bottom metallic layer to ensure zero transmission, and the rest of the structure comprising couple of layers, with different materials and sometimes patterns play the role of suppression of reflection. Blocking reflection is obtained by designing the structure to have impedance matching with the free-space [16].

The typical ideas for achieving broadband absorption are decreasing the quality factor of the resonance mode contributing to the absorption, or combining different adjacent resonances to build a broad resonance band as the qualitative effect of those consisting resonances.

As examples for the first approach, i.e. decreasing the quality factor, we can mention decreasing the quality factor of the Fabry-Perot cavity resonators. This happens by using highly lossy metals in the metal-insulator-metal configuration which provide a wideband impedance matching with free-space due to their appropriate optical properties, such as Mn [17] or Chromium (Cr) [18]. Decreasing the quality factor is also obtainable by using metal-insulator-metal-insulator configuration where the top insulator is added as an intermedial layer to make the impedance transition from air to the cavity more gradual [19,20]. This eventually leads to broadening the impedance matching band.

About the second approach which is gathering the superposition of adjacent resonances, we may refer to one of the pioneer works carried out by Aydin. et al [21]. In that work, they adopted the collective absorption effects of adjacent Localized Surface Plasmon (LSP) resonances caused by varying widths of metallic nanorods and obtained an average of 71% absorption in the range of 400-700 nm. Another example can be superposition of LSP resonances induced by randomly distributed nanoparticles on the top layer of an MIM configuration which leads to high absorption in the visible regime [22].

One huge barrier toward mass, large-area and high-throughput production of broadband absorbers is the costly and time-consuming stage of lithography. The typical used type of lithography is Electron Beam lithography (EBL). For the purpose of intuition, patterning a 1 cm² area of sample may take up to a several days. Therefore, this is a crucial limitation. As a result, coming up with lithography-free structures is of high importance for large-scale production [23].

Some of the implemented ideas for lithography-free broadband absorbers in previous works include Pt-coated randomly distributed chemically synthesized dielectric nanowires [24], high-temperature annealing of thin metallic layers to deform them into random nanoparticles or nanoholes [22,25,26], typical MIM or MIMI cavity-based absorbers [19], and random nanopillars [27].

In this work, we present a facile and straightforward approach for the fabrication of ultra-broadband lithography-free absorbers by a single thick Mn layer coated over a high-roughness substrate including randomly distributed and sized needle-like and sharp nanopylramids. The measured absorption using an integrating sphere confirms an average of 99% absorption in the ultra-broad range of 250-2500 nm, i.e. from UV to MIR. Simulations predict that the absorption above 90% regime should at least go above 10 microns, which means UV to FIR. It is explained that such a broadband absorption is due to the cooperative contribution of two key factors: electromagnetic field tapering owing to the tapered nature of the structure, and especially appropriate optical properties of Mn [28,29]. These physical characteristics attribute to the fact that the thick coated Mn single-layer surprisingly, not only blocks the transmission, but also suppresses the reflection. Such a result, to the best of our knowledge, is the best obtained with lithography-free structures. This concept can be generalized to high-roughness substrates with different materials, as well, because as mentioned, the field does not penetrate below the Mn layer and therefore, the substrate only is required to have tapered features on it, regardless of its constituent material. Such a desirable result with a feasible approach can be beneficial for mass production purposes with a variety of applications ranging from photovoltaics to thermal emission.

Result and Discussion

Figure 1(a) demonstrates the Scanning Electron Microscopy (SEM) image of the surface of a commercial p-type silicon wafer substrate with ultra-high-roughness texture on which randomly shaped, sized, and distributed pyramids exist. To achieve this feature, we have adopted a recipe of ICP with cyclic steps, using STS Multiplex ICP Etch system. Each step consists of two half steps of reactive ion etching (RIE) and deposition (passivation). In the first half step of RIE a mixture of SF₆ and O₂ gasses are released for a duration of 10 s and in the second half step of deposition, the gas of C₄F₈ gets deposited for 7 s. Gas flow

rate for SF₆, O₂ and C₄F₈ was set to 80, 5, and 70 sccm, respectively. The chamber pressure during the half steps of etching and deposition was set to 35 and 20 mTorr, respectively. During the etching and deposition half steps, the coil power was set to 500 and 400 Watts, respectively, and the platen power was set to 13 and 0 Watts, respectively. The chamber temperature was set to 20 C. The features shown in Fig. 1(a) were obtained by 300 cycles of the explained recipe. Based on our experiments, approximately after 100 cycles these features start to appear and increasing the number of the cycles increases the size of the random nanopylramids. As a tradeoff between the etching total time and relatively large and tall nanopylramids, we had set the number of cycles to 300 to keep the etching process relatively high-throughput. Using this method, we obtained such features on a full 4 inch Si wafer, therefore, this process is large-area and can be applied to any size of wafers. The image of the Si wafer after the etching is also shown in Fig. 1(b). It can be observed from Fig. 1(a) that the shaped pyramids are sharp and needle-like and they randomly vary in their size and distribution. The black color of the Si wafer in Fig. 1(b) is attributed to the high absorption of the nanopylramids of doped Si in the visible region. However, as will be shown later on, the absorption in this case is limited to the visible region and for larger wavelengths, the structure loses its high absorption behavior. In order to extensively broaden the perfect absorption band up to FIR, we coat a single layer of Mn with the thickness of 600 nm, using VAKSIS electron-beam evaporator system. The coating rate was set to 10 A/s. The relatively high rate of coating is due to the fact that in this work it is not required to have flat coatings, therefore, we can use high rates for coating for this work which is a positive feature for high-throughput production purposes.

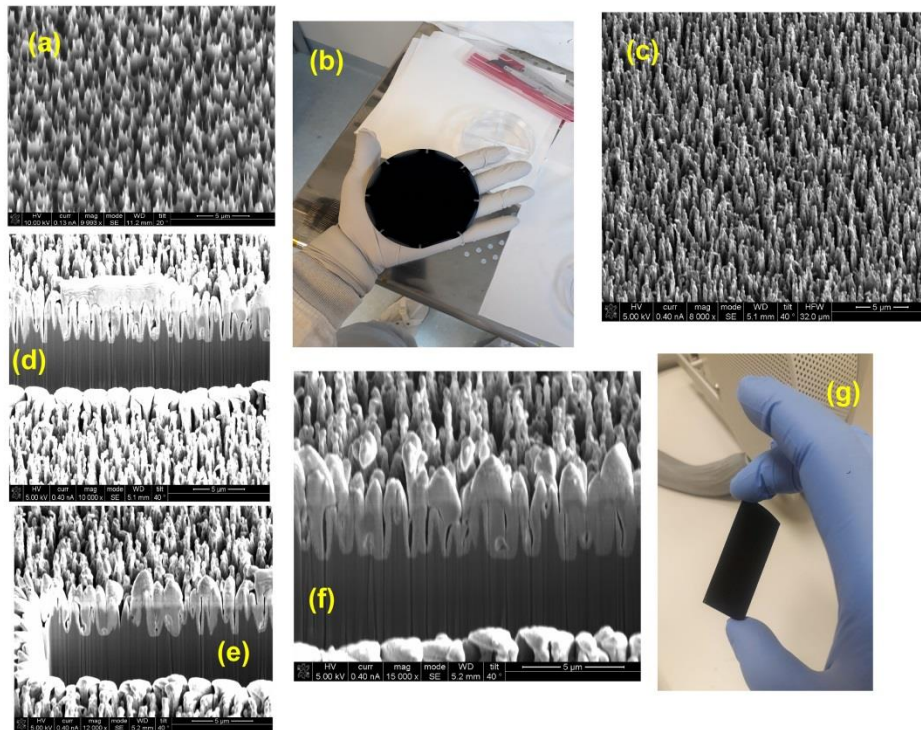


Figure 1. a) SEM image of the sample with high-roughness substrate before coating of Mn, b) image of the fabricated sample before coating of Mn, c) SEM image of the sample after coating of Mn, d,e,f) SEM images of the cross-section of the sample after coating of Mn, milled by FIB, g) image of the fabricated sample after coating of Mn

Figures 1(c-g) demonstrate the structure after coating of Mn. It is a well-known fact that coating such a high thickness of a metal layer suppresses the transmission completely, however, in this case, this coated single layer will not only suppress the transmission, but also the reflection in an ultra-wide range

spanning from UV to FIR. The physical mechanism behind this behavior is explained in detail in the next parts of the paper. By comparing Figs. 1(a) and 1(c), it can be obviously observed that after coating Mn, the pyramids retain their sharpness. Figures 1(d-f) demonstrate the cross-section of the structure milled by Focused Ion Beam (FIB). It can be clearly observed that a thick layer of Mn is coated over the nanopyramids. Therefore, we have Mn-coated random distribution of nanopyramids over the whole substrate. Fig. 1(g) also depicts image of the final sample after coating of Mn.

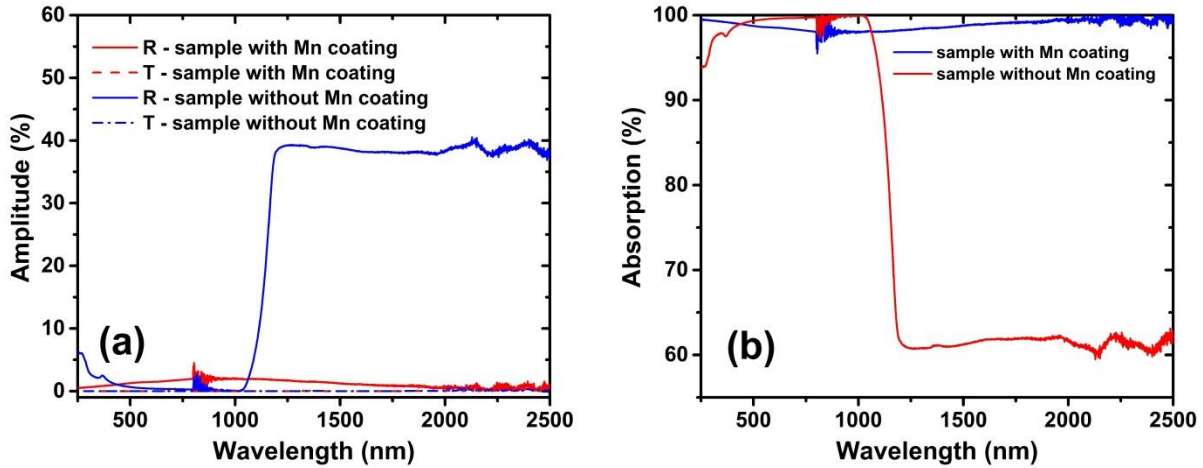


Figure 2. a) Reflection and transmission spectra of the high-roughness substrate with random nanopyramids for the cases of before and after coating of 600 nm Mn, b) absorption of the structure for the cases of before and after coating of Mn.

In order to measure the absorption (A) spectrum of such a structure, we have to measure the transmission (T) and reflection (R). Then the absorption can be calculated as: $A=1-R-T$. T can be measured by using normal devices such as ellipsometer or FTIR. However, for measuring R, we require an integrating sphere set up to be integrated with the device we are using. This is due to the fact that because of the nonplanar geometry of the structure, a high portion of the reflected wave will be scattered, i.e. we have to measure both diffusive and specular reflections from the sample. Any device without an integrating sphere setup only measures the specular reflection. For instance, for the case of normal incidence, only that portion of the reflection which directly comes back to the source is measured. However, the integrating sphere has a reflective mirror inside it and gathers all portions of the reflected beam which is scattered to any direction and sends all to the detector. The integrating sphere used in our device, is attached to the Carry 5000 UV-VIS-IR spectrophotometer and measures in the range of 250-2500 nm. Using this method, the measured reflection for the cases of before and after coating the Mn layer is shown in Fig. 2(a). Also the measured transmission using Fourier Transform Infrared (FTIR) is included in the same figure. From there, the experimental absorption spectrum is calculated and shown in Fig. 2(b) for both cases of before and after coating of Mn. It can be observed that before coating Mn, the structure has perfect absorption up to around 1000 nm wavelength and after that the absorption drops significantly. This is attributed to the tapered nature of the patterns along with the inherent loss of Si in this wavelength range, plus possible effects of doping material contributing to the absorption. About the sample after coating of Mn, it can be observed that the near-perfect absorption regime ranges from 250 to 2500 nm, i.e. from UV to MIR. The average absorption in the measured range is approximately 99%. Such a wideband absorption without the inclusion of lithography, has not been experimentally reported before, to the best of our knowledge. However, although the integrating sphere setup is limited up to the wavelength of 2500 nm, as it will be shown in the next sections, simulations confirm that the absorption band of the structure should go up to

around 10 microns, i.e. from UV to FIR. It is also evident from the trend of measured absorption behavior of the structure in Fig. 2(b) as the wavelength increases, that the absorption does not show a negative slope toward the larger wavelengths, and if the same trend continues for the larger wavelengths that have not been measured, the absorption will remain above 90% for up to a couple of microns larger than 2500 nm wavelength.

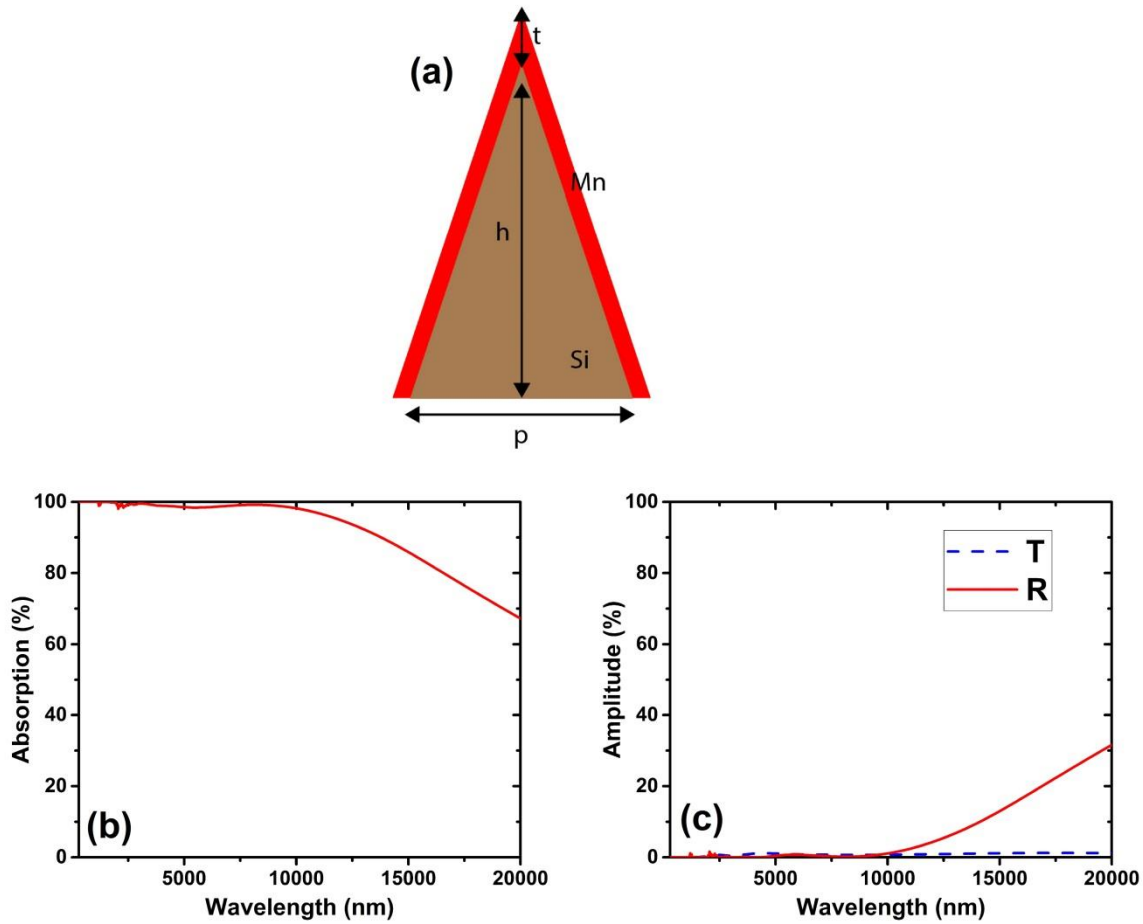


Figure 3. a) xz cross-section schematic of the unit cell of the approximated model of the structure, b) Calculated absorption spectrum of the structure when $h=4$, $p=1$, and $t=0.6$ microns, c) Calculated reflection and transmission spectra for the structure with the dimensions of (b)

Based on the Figs. 1(d-f) we can approximate the structure as periodic arrays of Mn-coated pyramids, the xz cross-section of the unit cell of which is shown in Fig. 3(a). As can be seen, the height of the inner pyramid made of Si, the period, and the thickness of the coated metal layer are denoted as h , p , and t , respectively. According to the SEM images taken from the cross-section of the sample, we choose $h=4$ microns, $p=1$ micron, and $t=600$ nm for the simulation. By choosing the unit cell as shown in Fig. 3(a) for our simulation, we define the boundary condition as periodic in the x and y directions. The absorption result of the approximated structure is shown in Fig. 3(b). Simulations are carried out using Lumerical FDTD commercial software. It is also noteworthy that the permittivity of Mn used throughout the paper is measured by fitting measured spectroscopy data obtained by J.A. Woollam Co. Inc. V-VASE and IR-VASE Ellipsometers. Also the material data of Si is taken from Palik. It can be observed that such a structure shows absorption of above 90% up to the wavelength of 13500 nm, i.e. spanning from UV to

FIR. To discuss the results more clearly, the reflection and transmission of this sample are shown in the same plot in Fig. 3(c). It can be observed that in the mentioned ultra-broad range, both the reflection and transmission are suppressed. The transmission is suppressed due to the high thickness of the Mn layer which is 600 nm, and reflection is suppressed because of the effect of Field Tapering. So, unlike previous structures in which the high thickness metallic layer is put at the bottommost part to only block the transmission, and the minimization of reflection happens due to the contribution of the other parts of the structure above the thick bottom layer, in our case, a thick metallic layer plays the role of blocking both the transmission and reflection at the same time without any need to other coatings on it. It is due to the tapered geometric shape of the substrate which enables the effect of field tapering. This effect, along with the very appropriate optical properties of Mn which will be discussed in detail later, contributes to such a broadband absorption.

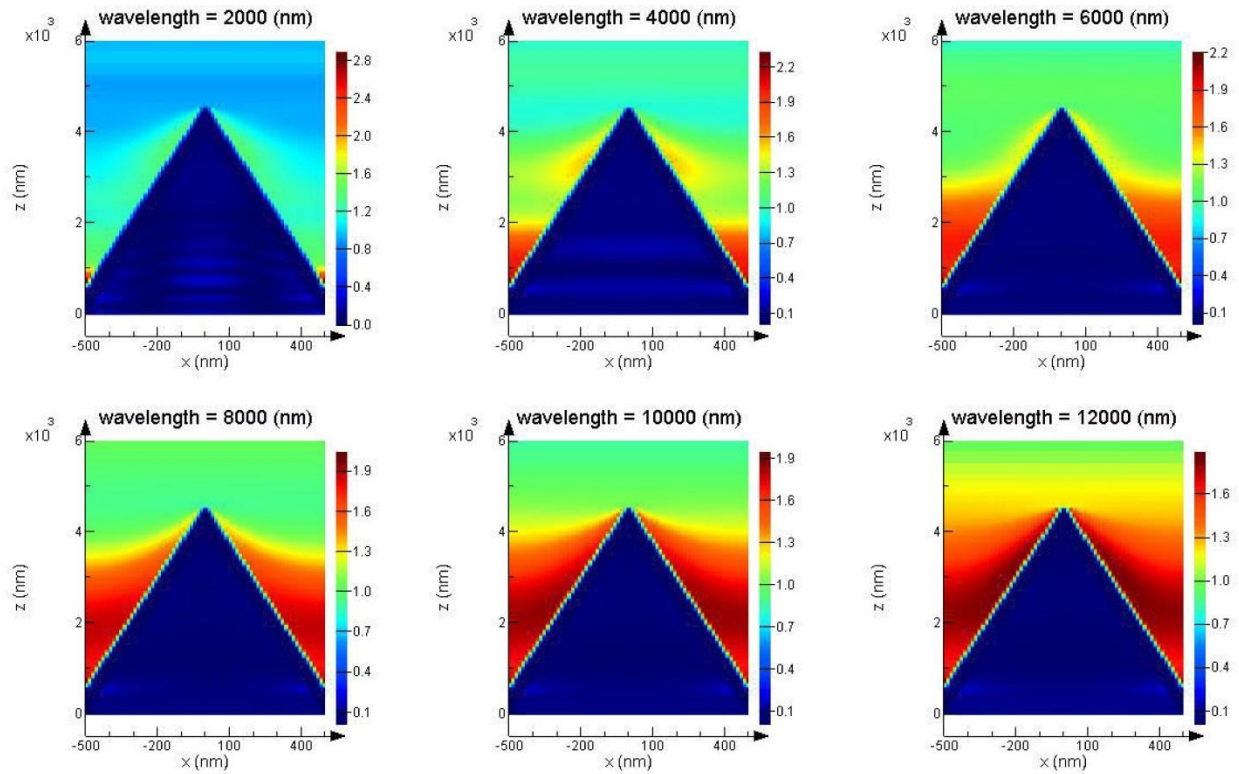


Figure 4. Electric field magnitude distribution at the xz cross-section of the unit cell for different wavelengths of 2, 4, 6, 8, 10, 12 microns.

Now, we discuss the physical mechanism behind this broadband absorption. As the first step toward physical analysis, the electric field magnitude pattern is shown at the xz-plane cross-section of the unit cell in Fig. 4. The simulations are carried out for the different wavelengths of 2, 4, 6, 8, 10 and 12 microns. The field patterns clearly demonstrate the effect of field tapering. Field tapering happens when there is a gradual and smooth impedance matching between the air and structure. Tapering can also be used as transformation optics for adjusting the wave-front width between two different sections of a structure with different widths. As mentioned, this happens by a gradual impedance matching between those two sections. In our case, also it can be observed in Fig. 4 that for different wavelengths, the position of field coupling to the structure varies slowly. This shows that the incident field slowly gets coupled to the structure in the region between the adjacent unit cells, but cannot penetrate inside the pyramids below the coated layer, because of the high thickness of the layer. After coupling slowly to the

structure, the field gets absorbed inside the Mn layer, by penetrating inside it (but not below it inside the pyramids).

Figure 5.(a) demonstrates the reflection spectrum for different coated metals, which are typically the best reported metals for broadband absorber structures. These metals include W, Cr, Ti, Fe, and Mn. The dimensions are as chosen before, i.e. $t=600$ nm, $p=1$ microns, and $h=4$ microns. It can be observed that for the case of other metals, the $R<10\%$ band at the best goes up to the wavelength of approximately 6.7 microns for the case of Ti, while when using Mn the bandwidth enhances very significantly and the upper wavelength limit of $R<10\%$ band goes up to around 13.5 microns. This significant superiority of Mn can be explored in its optical properties. For this purpose, we have plotted the real part of relative permittivity of all the metals in Fig. 5(b). The optical data for Mn is measured and for other metals it is taken from Palik. It can be observed that in such a broad wavelength range, Mn has a much smaller real part of permittivity compared to the other metals which retains its small value throughout the whole spectrum. Having a small real part of permittivity leads to high field penetration inside the metal and through the intrinsic loss of metal, i.e. the imaginary part of permittivity, the penetrated field gets absorbed.

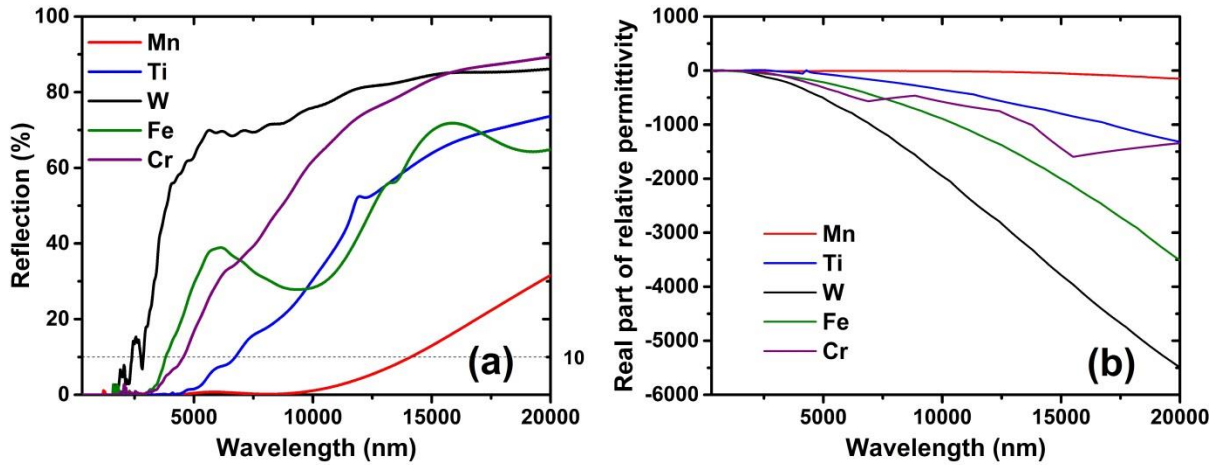


Figure 5. a) Reflection spectrum of the structure for different coated metals, b) Real part of relative permittivity of metals shown in (a).

Based on the abovementioned arguments it can be concluded that the main physical reasons behind this broadband strong absorption are: 1. The phenomena of field tapering which is due to the tapered nature of the structure components, and, 2. The significantly small real part of permittivity of Mn, which allows high field penetration inside itself and consequently leads to high absorption. As explained above, the field tapering effect couples the incident field to the structure in a broad wavelength range, and the coupled field penetrates easily inside the Mn layer and gets absorbed there. Thus, the absorptive behavior is a result of collective cooperation of the tapered structures along with the appropriate optical properties of Mn as the absorptive metal.

Conclusion

In summary, a facile and feasible lithography-free approach for obtaining ultra-broadband perfect absorption through a single layer coating of Manganese over a high-roughness substrate including random nanopylramids, is experimentally presented. The experimental measurements using integrating sphere confirm approximately 99% average absorption in the range of 250 to 2500 nm, i.e. from UV to MIR. The

simulations predict that the absorption band extends up to above 10 microns, in other words, from UV to FIR. The physical mechanism behind this broadband absorption is discussed and it is shown that this is due to the cooperative contribution of superior optical properties of Mn along with the phenomena of electromagnetic field tapering, which happens due to the tapered nature of the structure. The tapered structures on the surface of the substrate are obtained by ICP etching. However, this approach can be used for any high-roughness substrate with pyramidal-shaped features on it. The findings and experiments of this paper are very beneficial for large-area and mass production of broadband absorbers in the unprecedented range of UV to FIR.

References

1. D. P. McMeekin, G. Sadoughi, W. Rehman, G. E. Eperon, M. Saliba, M. T. Horantner, A. Haghighirad, N. Sakai, L. Korte, B. Rech, M. B. Johnston, L. M. Herz, and H. J. Snaith, "A mixed-cation lead mixed-halide perovskite absorber for tandem solar cells," *Science* **351**(6269), 151-155 (2016).
2. Z. Y. Wang, Z. Tong, Q. X. Ye, H. Hu, X. Nie, C. Yan, W. Shang, C. Y. Song, J. B. Wu, J. Wang, H. Bao, P. Tao, and T. Deng, "Dynamic tuning of optical absorbers for accelerated solar-thermal energy storage," *Nat Commun* **8**((2017).
3. L. Zhou, S. D. Zhuang, C. Y. He, Y. L. Tan, Z. L. Wang, and J. Zhu, "Self-assembled spectrum selective plasmonic absorbers with tunable bandwidth for solar energy conversion," *Nano Energy* **32**(195-200 (2017).
4. Q. Guo, G. M. Ford, H. W. Hillhouse, and R. Agrawal, "Sulfide Nanocrystal Inks for Dense $\text{Cu}(\text{In}_{1-x}\text{Ga}_x)(\text{S}_{1-y}\text{Se}_y)_2$ Absorber Films and Their Photovoltaic Performance," *Nano Lett* **9**(8), 3060-3065 (2009).
5. D. G. Cahill, P. V. Braun, G. Chen, D. R. Clarke, S. H. Fan, K. E. Goodson, P. Keblinski, W. P. King, G. D. Mahan, A. Majumdar, H. J. Maris, S. R. Phillpot, E. Pop, and L. Shi, "Nanoscale thermal transport. II. 2003-2012," *Appl Phys Rev* **1**(1)(2014).
6. W. Li and J. Valentine, "Metamaterial Perfect Absorber Based Hot Electron Photodetection," *Nano Lett* **14**(6), 3510-3514 (2014).
7. S. C. Song, Q. Chen, L. Jin, and F. H. Sun, "Great light absorption enhancement in a graphene photodetector integrated with a metamaterial perfect absorber," *Nanoscale* **5**(20), 9615-9619 (2013).
8. A. A. Bessonov, M. Allen, Y. L. Liu, S. Malik, J. Bottomley, A. Rushton, I. Medina-Salazar, M. Voutilainen, S. Kallioinen, A. Colli, C. Bower, P. Andrew, and T. Ryhanen, "Compound Quantum Dot-Perovskite Optical Absorbers on Graphene Enhancing Short-Wave Infrared Photodetection," *Acs Nano* **11**(6), 5547-5557 (2017).
9. S. A. Dereshgi, Z. Sisman, K. Topalli, and A. K. Okyay, "Plasmonically enhanced metal-insulator multistacked photodetectors with separate absorption and collection junctions for near-infrared applications," *Sci Rep-Uk* **7**((2017).
10. S. Mokkalapati, D. Saxena, H. H. Tan, and C. Jagadish, "Optical design of nanowire absorbers for wavelength selective photodetectors," *Sci Rep-Uk* **5**((2015).

11. I. E. Carranza, J. P. Grant, J. Gough, and D. Cumming, "Terahertz Metamaterial Absorbers Implemented in CMOS Technology for Imaging Applications: Scaling to Large Format Focal Plane Arrays," *Ieee J Sel Top Quant* **23**(4)(2017).
12. K. B. Fan, J. Y. Suen, X. Y. Liu, and W. J. Padilla, "All-dielectric metasurface absorbers for uncooled terahertz imaging," *Optica* **4**(6), 601-604 (2017).
13. N. I. Landy, C. M. Bingham, T. Tyler, N. Jokerst, D. R. Smith, and W. J. Padilla, "Design, theory, and measurement of a polarization-insensitive absorber for terahertz imaging," *Phys Rev B* **79**(12)(2009).
14. T. C. Cao, K. L. Xu, G. M. Chen, and C. Y. Guo, "Poly(ethylene terephthalate) nanocomposites with a strong UV-shielding function using UV-absorber intercalated layered double hydroxides," *Rsc Adv* **3**(18), 6282-6285 (2013).
15. T. Khalid, L. Albasha, N. Qaddoumi, and S. Yehia, "Feasibility Study of Using Electrically Conductive Concrete for Electromagnetic Shielding Applications as a Substitute for Carbon-Laced Polyurethane Absorbers in Anechoic Chambers," *Ieee T Antenn Propag* **65**(5), 2428-2435 (2017).
16. N. Mattiucci, M. J. Bloemer, N. Akozbek, and G. D'Aguanno, "Impedance matched thin metamaterials make metals absorbing," *Sci Rep-Uk* **3**((2013).
17. M. Aalizadeh, A. Khavasi, B. Butun, and E. Ozbay, "Large-Area, Cost-Effective, Ultra-Broadband Perfect Absorber Utilizing Manganese in Metal-Insulator-Metal Structure," *Sci Rep-Uk* **8**((2018).
18. Z. Y. Li, E. Palacios, S. Butun, H. Kocer, and K. Aydin, "Omnidirectional, broadband light absorption using large-area, ultrathin lossy metallic film coatings," *Sci Rep-Uk* **5**((2015).
19. S. A. Dereshgi, A. Ghobadi, H. Hajian, B. Butun, and E. Ozbay, "Ultra-Broadband, Lithography-Free, and Large-Scale Compatible Perfect Absorbers: The Optimum Choice of Metal layers in Metal-Insulator Multilayer Stacks," *Sci Rep-Uk* **7**((2017).
20. M. Chirumamilla, A. S. Roberts, F. Ding, D. Y. Wang, P. K. Kristensen, S. I. Bozhevolnyi, and K. Pedersen, "Multilayer tungsten-alumina-based broadband light absorbers for high-temperature applications," *Opt Mater Express* **6**(8), 2704-2714 (2016).
21. K. Aydin, V. E. Ferry, R. M. Briggs, and H. A. Atwater, "Broadband polarization-independent resonant light absorption using ultrathin plasmonic super absorbers," *Nat Commun* **2**((2011).
22. S. A. Dereshgi and A. K. Okyay, "Large area compatible broadband superabsorber surfaces in the VIS-NIR spectrum utilizing metal-insulator-metal stack and plasmonic nanoparticles," *Opt Express* **24**(16), 17644-17653 (2016).
23. M. Aalizadeh, A. E. Serebryannikov, A. Khavasi, G. A. E. Vandenbosch, and E. Ozbay, "Toward Electrically Tunable, Lithography-Free, Ultra-Thin Color Filters Covering the Whole Visible Spectrum," *Sci Rep-Uk* **8**((2018).
24. A. Ghobadi, S. A. Dereshgi, H. Hajian, G. Birant, B. Butun, A. Bek, and E. Ozbay, "97 percent light absorption in an ultrabroadband frequency range utilizing an ultrathin metal layer: randomly oriented, densely packed dielectric nanowires as an excellent light trapping scaffold," *Nanoscale* **9**(43), 16652-16660 (2017).

25. A. Ghobadi, S. A. Dereshgi, H. Hajian, B. Bozok, B. Butun, and E. Ozbay, "Ultra-broadband, wide angle absorber utilizing metal insulator multilayers stack with a multi-thickness metal surface texture," *Sci Rep-Uk* **7**((2017).
26. A. Ghobadi, H. Hajian, S. A. Dereshgi, B. Bozok, B. Butun, and E. Ozbay, "Disordered Nanohole Patterns in Metal-Insulator Multilayer for Ultra-broadband Light Absorption: Atomic Layer Deposition for Lithography Free Highly repeatable Large Scale Multilayer Growth," *Sci Rep-Uk* **7**((2017).
27. M. Chirumamilla, A. Chirumamilla, Y. Q. Yang, A. S. Roberts, P. K. Kristensen, K. Chaudhuri, A. Boltasseva, D. S. Sutherland, S. I. Bozhevolnyi, and K. Pedersen, "Large-Area Ultrabroadband Absorber for Solar Thermophotovoltaics Based on 3D Titanium Nitride Nanopillars," *Adv Opt Mater* **5**(22)(2017).
28. M. Aalizadeh, A. Khavasi, A. E. Serebriyannikov, G. A. E. Vandenbosch, and E. Ozbay, "A Route to Unusually Broadband Absorption Spanning from Visible to Mid-Infrared," arxiv preprint, 1810.07139 (2018).
29. M. Aalizadeh, A. Khavasi, B. Butun, and E. Ozbay, "Lithography-Free, Manganese-Based Ultra-Broadband Absorption Through Annealing-Based Deformation of Thin Layers into metal-air composites," arxiv preprint, 1810.07136 (2018).